NUCL SCI TECH (2019) 30:15
https://doi.org/10.1007/s41365-018-0534-6

Yield ratios and directed flows of light particles from proton-rich nuclei-induced collisions

Ting-Zhi Yan[1] · Shan Li[1] · Yan-Nan Wang[1] · Fei Xie[1] · Ting-Feng Yan[2]

Received: 1 March 2018 / Revised: 24 September 2018 / Accepted: 1 October 2018 / Published online: 2 January 2019

Abstract The neutron-to-proton and ^{3}H-to-^{3}He yield ratios, and the directed flows of particles dependent on a reduced rapidity, the transverse momentum per nucleon, and a reduced impact parameter are investigated for ^{28}S + ^{28}Si and ^{32}S + ^{28}Si systems at 50 and 400 MeV/u using an isospin-dependent quantum molecular dynamics model. The results show that these yield ratios of projectile-like fragments are approximately equal to the constituent neutron-to-proton ratio of the projectile. There are clear differences of the directed flows for isospin-related fragments neutron and proton, ^{3}H and ^{3}He from ^{28}S + ^{28}Si collisions. The differences in directed flows for neutrons and protons and ^{3}H–^{3}He from a proton-rich nucleus ^{28}S− induced collisions are noticeably larger than those from a stable nucleus ^{32}S− induced reactions under medium impact parameters. Thus, the yield ratios and differences in directed flows for the neutrons and protons and ^{3}H–^{3}He under medium impact parameters are proposed as possible observable items for studying isospin physics.

Keywords Yield ratio · Directed flow · Proton-rich nucleus

This work was supported by the National Natural Science Foundation of China (No. 11405025).

✉ Ting-Zhi Yan
ytz0110@163.com

1 School of Energy and Power Engineering, Northeast Electric Power University, Jilin 132012, China

2 State Grid Tancheng Power Supply Company, Linyi 276100, China

1 Introduction

The properties of nuclei near a beta-stable line including the nuclear structure and reactions have been well known through decades of effort by various scientists. The characteristics of exotic nuclei near neutron and proton drip lines have gradually attracted attention since Tanihata first found the neutron-halo structure of ^{11}Li, and a large number of radioactive ion beam facilities have been built in many national laboratories in recent years. As the most important structural behavior of a neutron-rich nucleus, the neutrons have much more extended density distributions than the protons, i.e., a neutron skin or halo, which can be applied by certain theoretical models of nuclear structures, such as the relativistic-mean-field [1–4], Skyrme–Hartree–Fock [5–7], and shell models [8–10]. It also has some other properties such as a small separation energy, low angular momentum on the orbits of the last few nucleons, and an increased reaction cross section, which can be measured experimentally [11–14]. However, studies have mostly focused on neutron skins and halos, with fewer studies conducted on proton skins and halos, and the experimental approaches used to study exotic nuclei must be expanded to include the isospin. Directed and elliptical flows have been identified as sensitive observables with regard to the isospin effect in equations of state for nuclear matter and the dynamics of nuclear collisions [15–20]; for instance, neutron-rich systems have a higher balance energy (at which the in-plane transverse flow disappears) compared to neutron-deficient systems for all colliding parameters [20], and the isospin dependence of collective flows has been explained as competition among various isospin-dependent reaction mechanisms including nucleon–nucleon collisions, symmetry energy, the surface property of the colliding nuclei, and the Coulomb force. The yield ratio of neutrons to protons has also been proposed as a candidate to investigate the isospin physics, such as the symmetry energy at subnormal and supranormal densities, isospin splitting of the nucleon effective mass, and an in-medium nucleon–nucleon cross section [21–30]. However, such studies have mostly focused on neutron-rich nuclei-induced collisions, with a lack of research conducted on reactions induced through proton-rich nuclei. In this work, the yield ratios and directed flows of light particles from proton-rich nucleus ^{28}S$-$ induced reactions ^{28}S + ^{28}Si at 50 and 400 MeV/u are explored, and stable isotopic nuclei ^{32}S$-$ induced collisions ^{32}S + ^{28}Si are used for comparison.

2 Theoretical descriptions

The dynamics of heavy ion reactions should consist of three components: propagation of nucleons in the mean field, nucleon–nucleon collisions in a nuclear medium, and Pauli blocking. The quantum molecular dynamics (QMD) model is a successful many-body theory that can explicitly describe the state of a reaction system and can represent the time evolution of the colliding system extremely well from intermediate to relativistic energies. A detailed review of the QMD model can be found in Ref. [31]. The isospin-dependent quantum molecular dynamics (IQMD) model is based on the above theory, affiliated with the isospin effect on the above three constituents [32, 33].

The nuclear mean-field potential used in the IQMD model can be parameterized as follows [32, 33]:

$$U(\rho,\tau_z)=\alpha\left(\frac{\rho}{\rho_0}\right)+\beta\left(\frac{\rho}{\rho_0}\right)^{\gamma}+\frac{1}{2}(1-\tau_z)V_{\mathrm{c}} + C_{\mathrm{sym}}\frac{(\rho_{\mathrm{n}}-\rho_{\mathrm{p}})}{\rho_0}\tau_z+U^{\mathrm{Yuk}}, \tag{1}$$

where ρ_0 is the normal nuclear matter density ($0.16\,\mathrm{fm}^{-3}$); ρ, ρ_{p}, and ρ_{n} are the total, proton, and neutron densities, respectively; and τ_z is the zth constituent of the isospin degree of freedom, which equals 1 or -1 for neutrons or protons, respectively. The different parameters α, β, and γ represent the different nuclear equations of state. In addition, C_{sym} is the symmetry energy strength owing to the asymmetry of the neutrons and protons in the nucleus. In this work, $C_{\mathrm{sym}} = 32$ MeV is used. Here, V_{c} is the Coulomb potential and U_{Yuk} is the Yukawa (surface) potential. In the present study, we also adopt $\alpha = -356\,\mathrm{MeV}$, $\beta = 303\,\mathrm{MeV}$, and $\gamma = 1.17$, corresponding to the so-called soft EOS with an incompressibility of $K = 200\,\mathrm{MeV}$.

In the IQMD model, clusters emitted during a collision are usually distinguished through a coalescence method: When the two nucleons in a phase space satisfy a spatial distance Δr of smaller than 3.5 fm and a momentum difference Δp of smaller than 300 MeV/c, they can be treated as a part of a cluster [31, 34]. With this simple coalescence method, different sized clusters can be recognized, which has been extensively applied in transport theory for a cluster formation.

The nucleon–nucleon cross section used in this model is an experimental parametrization, which is also isospin-dependent. The cross section between a neutron and proton is about 3 times bigger than that between a neutron and neutron, or proton and proton, when the collision energy is below 300 MeV/u.

3 Results and discussion

Approximately 300, 000 collisions are simulated for ^{28}S + ^{28}Si and ^{32}S + ^{28}Si with soft EOS at 50 and 400 MeV/u, respectively. In this study, the physical information of the projectile-like particles is extracted at $200\,\mathrm{fm}/c$.

For the initialization of the nucleons of a projectile and target, the protons and neutrons are distinguished in the IQMD model, and the stability of the initialization sample must be tested. The Skyrme–Hartree–Fock (SHF) theory is used to determine the neutron and proton density distributions of the projectile and target nuclei. The proton (dot), neutron (dash), and total matter (solid) densities of ^{28}S and ^{32}S, given by the SHF method, are shown in the left and right panels of Fig. 1, respectively. It can be observed that an apparent proton skin exists in ^{28}S [1, 35], but not in ^{32}S.

The upper panel of Fig. 2 shows the reduced impact parameter (b_{re}) dependence of the proton-to-neutron (n/p, solid square) and ^{3}H-to-^{3}He (^{3}H/^{3}He, solid circle) yield ratios from a ^{28}S + ^{28}Si system at 50 MeV/u, where the hollow symbols are for the corresponding fragments from

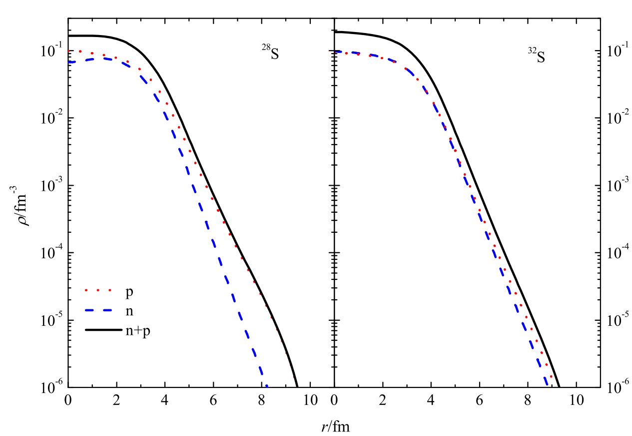

Fig. 1 (Color online) Neutron (dashed line), proton (dotted line), and total matter (solid line) density distributions of ^{28}S and ^{32}S given by the Skyrme–Hartree–Fock method

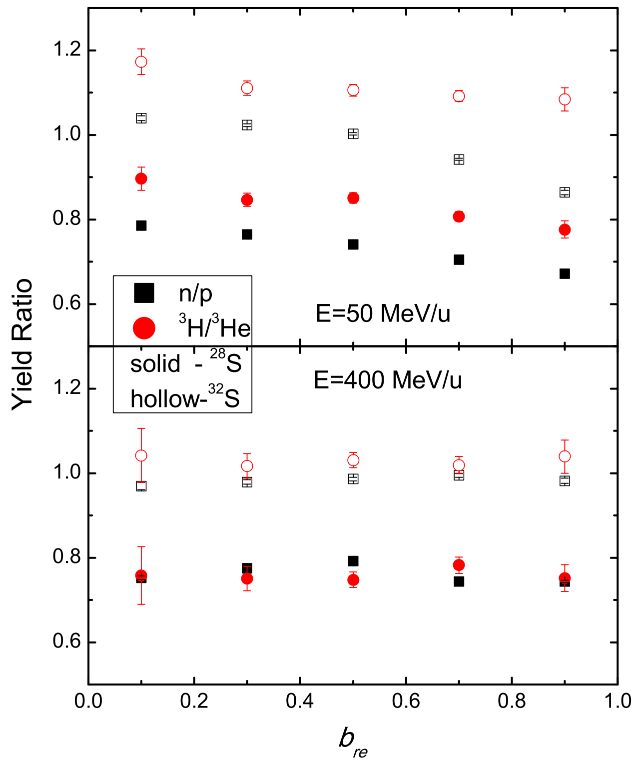

Fig. 2 (Color online) The reduced impact parameter dependence of the neutron-to-proton (square) and ^{3}H-to-^{3}He (circle) yield ratios from $^{28}S + ^{28}Si$ (solid symbols) and $^{32}S + ^{28}Si$ (hollow symbols) at 50 (upper panel) and 400 MeV/u (lower panel)

the $^{32}S + ^{28}Si$ system. Here, $b_{re} = b/b_{max}$, where b_{max} is the total radii of the projectile and target nuclei. The yield ratios of n/p and $^3H/^3He$ both decrease slightly with the reduced impact parameter for the attracting mean field and Coulomb effect within this energy range. The average ratios of n/p and $^3H/^3He$ are roughly evaluated to be 1.0 and 1.1, respectively, for the $^{32}S + ^{28}Si$ system and 0.75 and 0.85, respectively, for the $^{28}S + ^{28}Si$ system. The ratios of constituent neutrons to protons (N/P) of the two projectiles ^{32}S and ^{28}S are 1.0 and 0.75, respectively, which nearly coincide with the above yield ratios of the projectile-like fragments. This is a consequence of the coalescence method used in the IQMD model, and the emission probability of projectile-like particles should be proportional to the emission probabilities of their constituent nucleons. Thus, the yield ratio of $^3H/^3He$ should be close to that of n/p. The reason why the ratio of $^3H/^3He$ is larger than that of n/p may be because the larger charge of ^{3}He causes a much lower yield in low-energy collisions in which the attractive mean field plays a critical role. The lower panel of Fig. 2 shows the same correlation but for a collision energy of 400 MeV/u. It can be observed that the yield ratios of both n/p and $^3H/^3He$ are nearly unchanged with the reduced impact parameter because nucleon–nucleon collisions play a dominant role within this energy range. The yield ratios of n/p and $^3H/^3He$ are nearly equal for a certain collision system; in other words, they are both approximately 1.0 for the $^{32}S + ^{28}Si$ system and approximately 0.75 for the $^{28}S + ^{28}Si$ system, which is coincident with the N/P ratio of the projectile nucleus. Therefore, the yield ratios of n/p and $^3H/^3He$ can be used as isospin-dependent observables for investigating the reaction dynamics induced through a proton-rich nucleus.

The transverse collective flows carry important information regarding the pressure gradient, which builds up in the compressed zone, and are a direct way to the study the nuclear EOS. The invariant azimuthal distribution of the emitted fragments can be stated in the form of a Fourier expansion, as described below:

$$\frac{dN}{d\phi} \propto 1 + 2\sum_{n=1}^{\infty} v_n \cos(n\phi). \tag{2}$$

Here, ϕ is the azimuthal angle, which is defined as the angle between the particle's transverse momentum and the collision plane, labeled as the $x-z$ plane, whereas the beam direction is defined as the z-axis of the coordinate system, and the collision parameter direction is the x-axis. The so-called directed flow is the first harmonic coefficient v_1, which is expressed as follows:

$$v_1 = \langle \cos\phi \rangle = \left\langle \frac{p_x}{p_t} \right\rangle, \tag{3}$$

where p_t ($p_t = \sqrt{p_x^2 + p_y^2}$) is the transverse momentum of a fragment. The directed flow is dependent on the transverse momentum, rapidity, and other factors, and herein the rapidity is commonly used as the reduced rapidity in a center-of-mass frame, i.e., $y = y/y_{p_{c.m.}}$, where y_p is the rapidity of a projectile.

We show the scaled rapidity dependence of directed flows for neutrons and protons in a different centrality from $^{28}S + ^{28}Si$ and $^{32}S + ^{28}Si$ for the collisions at 50 and 400 MeV/u shown in Fig. 3. The directed flow at mid-rapidity ($0<y<0.5$) is negative for collisions at 50 MeV/u, but positive for those at 400 MeV/u, which is because the attractive mean field and rotation effect of the overlap zone play an important role in 50 MeV/u collisions, whereas the compulsive nucleon–nucleon collisions and expansion of the overlap zone play a dominant role at 400 MeV/u. Looking at the various panels in Fig. 3, there is a large similarity of the data in the different centralities. It can be observed that there are clear differences between the neutron and proton directed flows from $^{28}S + ^{28}Si$ collisions at 50 MeV/u, i.e., the absolute strength of v_1 in a proton is clearly larger than that in a neutron, which may be because protons have a positive symmetric potential,

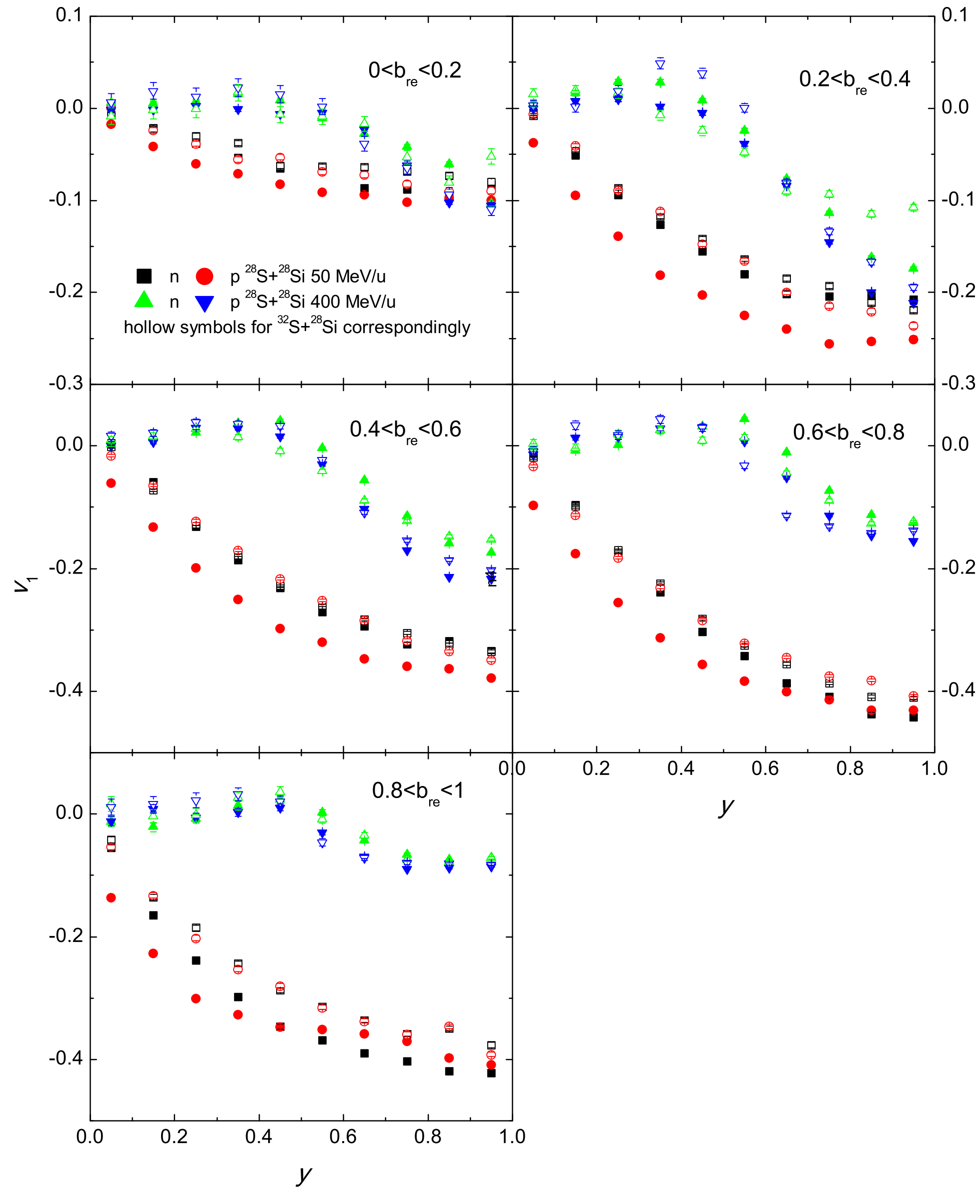

Fig. 3 (Color online) The reduced rapidity dependence of directed flows at a different centrality. The solid squares and circles indicate neutrons and protons from ^{28}S + ^{28}Si at 50 MeV/u, the solid upward and downward triangles indicate neutrons and protons from ^{28}S + ^{28}Si at 400 MeV/u, and the hollow upward and downward triangles indicate neutrons and protons from ^{32}S + ^{28}Si at 50 and 400 MeV/u, respectively

whereas neutrons have negative symmetric potential in ^{28}S; in other words, protons in a larger attractive mean field are emitted with a stronger directed flow. Thus, for the ^{32}S + ^{28}Si system, the directed flows of protons and neutrons are nearly equal to each other. For a similar reason, at high energy where compulsive nucleon–nucleon collisions play a dominant role, the neutrons should have a larger v_1 than the protons for ^{28}S + ^{28}Si collisions at 400 MeV/u, which we can also observe in Fig. 3, although not so clearly, for a small value of v_1 at this energy level.

The directed flows of isospin-related fragments ^{3}H and ^{3}He are also investigated, as shown in Fig. 4, for ^{28}S + ^{28}Si and ^{32}S + ^{28}Si at 50 MeV/u; however, no data are available for 400 MeV/u collisions owing to such small yields of ^{3}H and ^{3}He from such small impact systems at such a high collision energy. It can be observed that ^{3}He has a stronger directed flow than ^{3}H, which is similarly due to more protons and fewer neutrons present in ^{3}He.

The differential transverse momentum per nucleon (p_t/A) dependence of a directed flow limited in terms of the mid-rapidity interval $0 < y < 0.5$ for a neutron and proton in a different centrality from ^{28}S + ^{28}Si and ^{32}S + ^{28}Si in collisions at 50 and 400 MeV/u is shown in Fig. 5. The figure also shows that the directed flows of neutrons and protons are negative at 50 MeV/u and positive at 400 MeV/u for the same reason discussed above and that a change of v_1 occurs at 50 MeV/u after reaching the extremum, which may be due to the shadow effect of the spectators. Similarly, the absolute strength of v_1 of a proton is larger than that of a neutron from ^{28}S + ^{28}Si collisions at

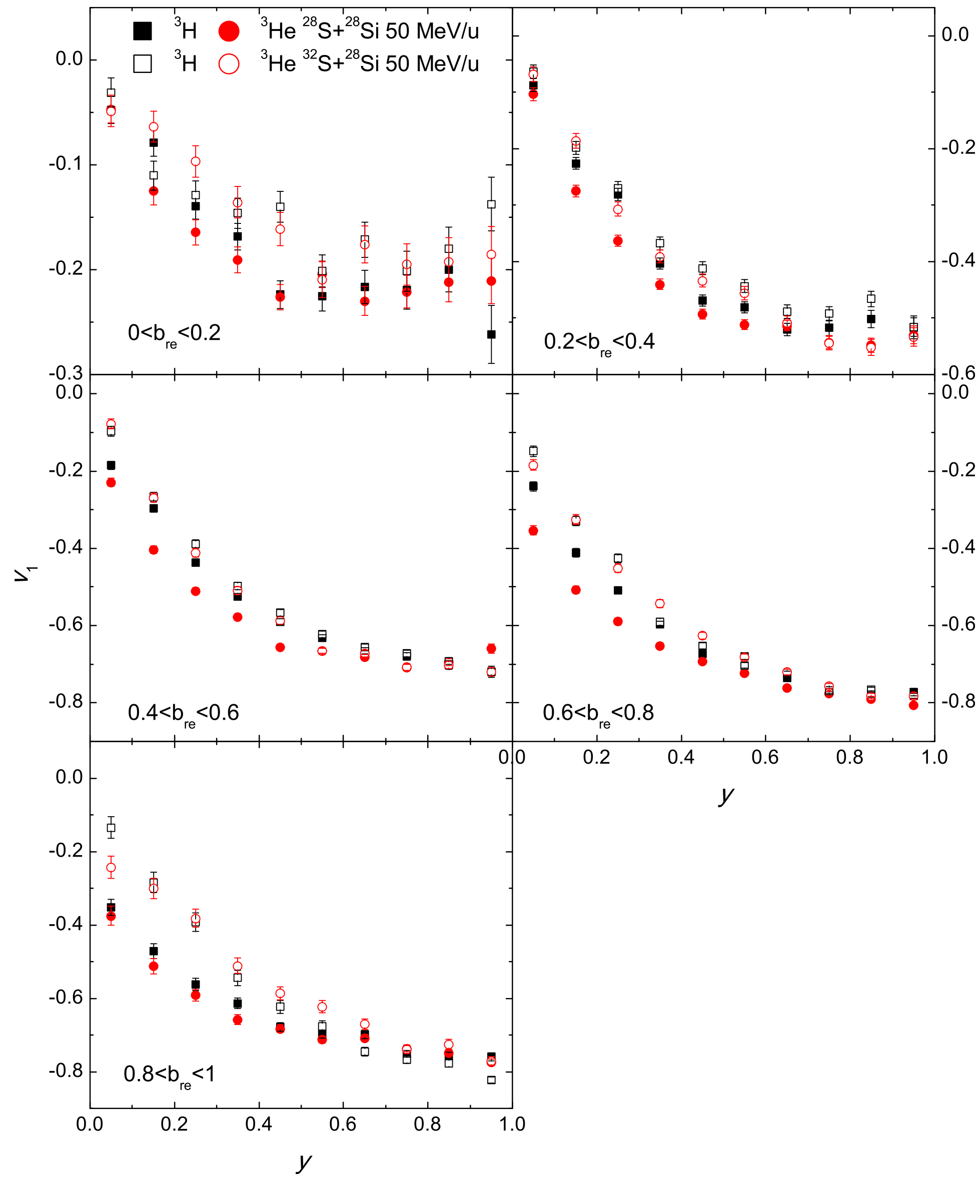

Fig. 4 (Color online) Reduced rapidity dependence of directed flows at a different centrality. The solid squares and circles indicate ^{3}H and ^{3}He from ^{28}S + ^{28}Si at 50 MeV/u, and the hollow squares and circles indicate ^{3}H and ^{3}He from ^{32}S + ^{28}Si at 50 MeV/u, respectively

50 MeV/u, whereas the absolute strength of v_1 of a proton is smaller (although not so clearly so) than that of a neutron for 400 MeV/u ^{28}S + ^{28}Si collisions. Figure 6 shows the same results as Fig. 5 but for fragments ^{3}H and ^{3}He at 50 MeV/u, and no data are available for 400 MeV/u collisions for the low yields of ^{3}H and ^{3}He. This indicates that ^{3}He has a stronger directed flow than ^{3}H, particularly in the middle centrality.

To quantitatively compare the difference between the isospin-related fragments and reduce the statistical error, the reduced impact parameter dependence of the directed flows integrated over $0 < y < 0.5$ and $p_t/A < 0.15$ GeV/A is determined. The upper panel of Fig. 7 shows the reduced impact parameter dependence of the directed flows of neutrons and protons from collisions at 50 MeV/u ^{28}S + ^{28}Si and ^{32}S + ^{28}Si. It can be observed that the integrated directed flows of neutrons and protons are both negative owing to the attractive mean field playing a dominant role at this low energy. The absolute values, i.e., the strength of directed flows of neutrons and protons, increase continuously with the reduced impact parameter for which the accompanied rotation effect also increases. This also indicates that the strength of v_1 of a proton is clearly larger, as mentioned above, than that of a neutron from a ^{28}S + ^{28}Si reaction system; however, for ^{32}S + ^{28}Si, there is no significant difference between protons and neutrons. Similar phenomena exist for ^{3}H and ^{3}He, as shown in the middle panel labeled with upward and downward triangles, respectively, i.e., ^{3}He has a stronger v_1 than ^{3}H for a ^{28}S + ^{28}Si system, although no clear distinction exists for a ^{32}S + ^{28}Si system. To quantify their distinctions,

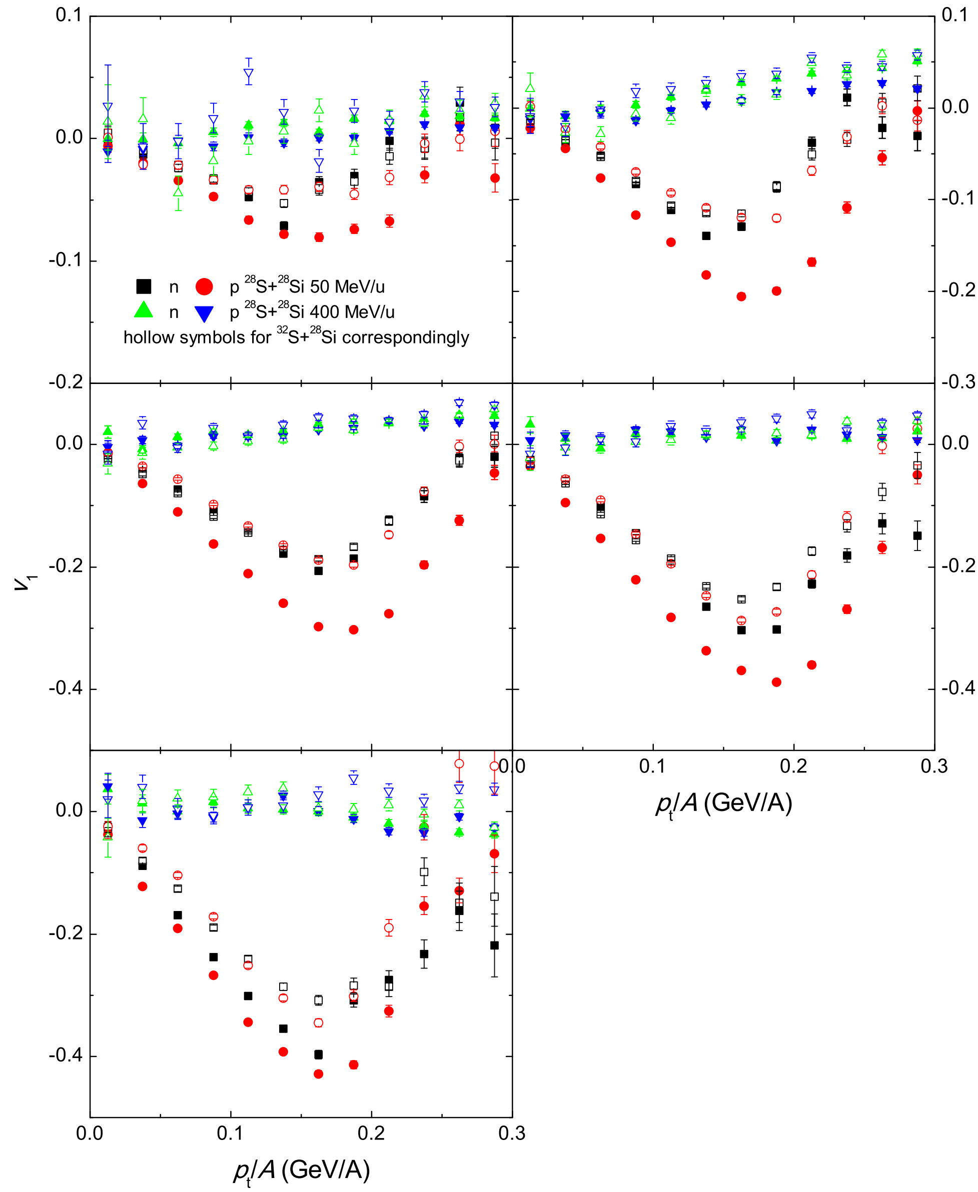

Fig. 5 (Color online) Similar to Fig. 3 but for transverse momentum per nucleon (p_t/A) dependence. The scaled rapidity is selected as $0<y<0.5$

the differences in v_1 ($\triangle v_1$) for neutron–proton (v_1(n)-v_1(p)) and ^{3}H–^{3}He ($v_1(^3\mathrm{H}) - v_1(^3\mathrm{He})$) are determined, as shown in the lower panel of Fig. 7. The figure indicates that the differences for neutron–proton and ^{3}H–^{3}He are noticeable and are nearly equal to each other for $^{28}\mathrm{S} + {}^{28}\mathrm{Si}$, and larger at intermediate impact parameters; however, they are extremely small and fluctuate at near zero for $^{32}\mathrm{S} + {}^{28}\mathrm{Si}$ within all collision parameters.

The results shown in Fig. 8 are similar to those in Fig. 7 but at an impact energy of 400 MeV/u. It can be observed that the directed flows of the light particles (shown in the upper and middle panels) are positive because nucleon–nucleon collisions and the expansion of the overlap zone play a dominant role at 400 MeV/u, and because the directed flows increase with a reduced impact parameter, but decrease in peripheral collisions, which may be due to the decreasing compression energy and gradient in the overlap zone. It can also be observed that neutrons have a clearly larger v_1 than protons from $^{28}\mathrm{S} + {}^{28}\mathrm{Si}$ reactions, which may be because neutrons own a weaker mean-field potential for a negative symmetric potential, and are emitted with stronger directed flow during expansion. The differences in v_1 for neutron–proton and ^{3}H–^{3}He are also presented in the lower panel of Fig. 8. The figure indicates that only the difference in neutron–proton from the $^{28}\mathrm{S} + {}^{28}\mathrm{Si}$ system is relatively noticeable and is larger for intermediate impact parameters, but much smaller than that from 50 MeV/u $^{28}\mathrm{S} + {}^{28}\mathrm{Si}$, and that the difference in n-p from a $^{32}\mathrm{S} + {}^{28}\mathrm{Si}$ system is extremely small, reaching approximately zero, whereas the differences in ^{3}H–^{3}He from the two reaction systems

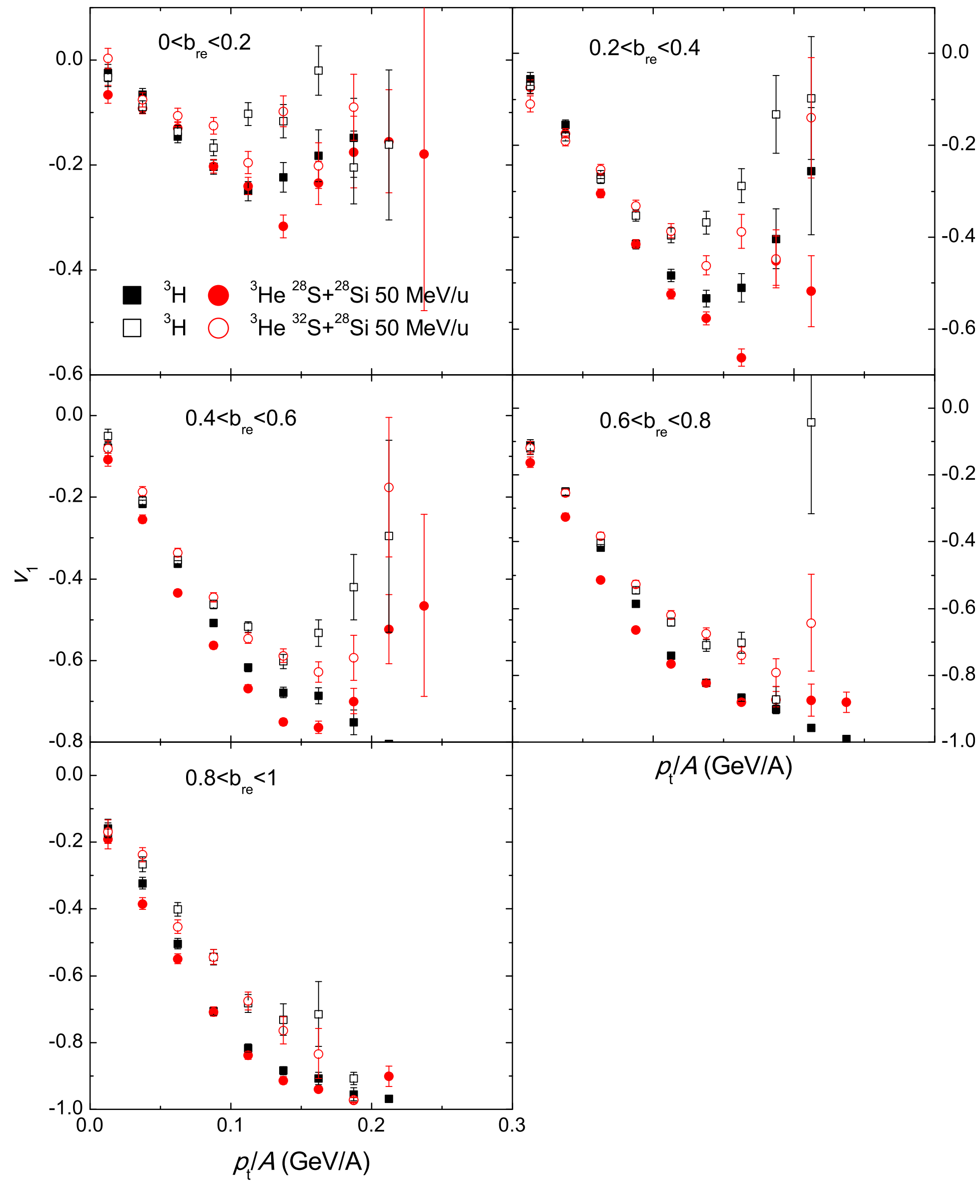

Fig. 6 (Color online) Similar to Fig. 4 but for transverse momentum per nucleon (p_t/A) dependence. The scaled rapidity is selected as $0 < y < 0.5$

fluctuate significantly owing to the small yields of ^{3}H and ^{3}He; in addition, the average value is also approximately zero within all collision parameters. Thus, from the previous analysis, the differences in directed flows for neutron–proton and ^{3}H–^{3}He can also represent isospin physics, and it is recommended to measure these physical quantities at low energies to obtain a larger value.

4 Summary

Using the IQMD model, we studied the rapidity and transverse momentum-dependent directed flows of projectile-like neutrons, protons, ^{3}H, and ^{3}He within full collision parameters for simulations of ^{28}S + ^{28}Si and ^{32}S + ^{28}Si at 50 and 400 MeV/u; in addition, the differences in v_1 for neutron–proton and ^{3}H–^{3}He, and the yield ratios of these light particles from the two reaction systems, were also investigated. It was also demonstrated that the yield ratios of n/p and ^{3}H/^{3}He for projectile-like fragments from low-energy collisions slightly decrease with reduced impact parameters, but are on average equal to the constituent N/P ratio of the projectile nuclei, whereas they are both nearly equal to the N/P of the projectile nuclei within all reduced impact parameters for high-energy collisions. The detailed characteristics of this may depend on the different parameters of the EOS, collision system, and other factors, requiring further theoretical research. The differences in

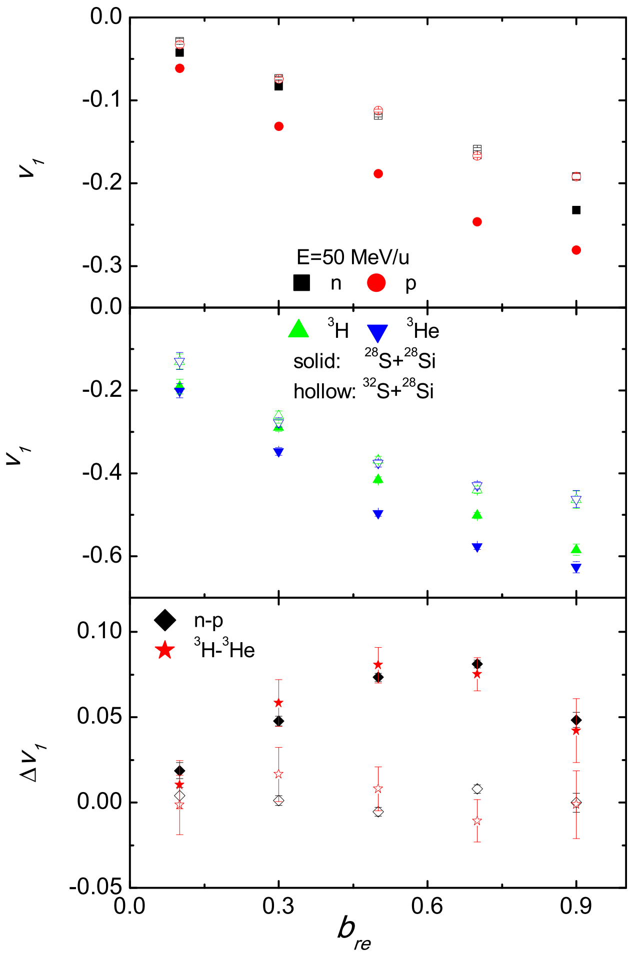

Fig. 7 (Color online) Upper and middle panels: directed flows dependent on reduced impact parameter. The squares, circles, upward triangles, and downward triangles indicate neutrons, protons, ^{3}H, and ^{3}He, respectively. Lower panel: the differences in v_1 (Δv_1) dependent on a reduced impact parameter. The diamonds and stars indicate $v_1(n)$-$v_1(p)$ (n-p) and $v_1(^3\mathrm{H})$-$v_1(^3\mathrm{He})$ (^{3}H–^{3}He), respectively. The solid and hollow symbols indicate ^{28}S + ^{28}Si and ^{32}S + ^{28}Si at 50 MeV/u, respectively

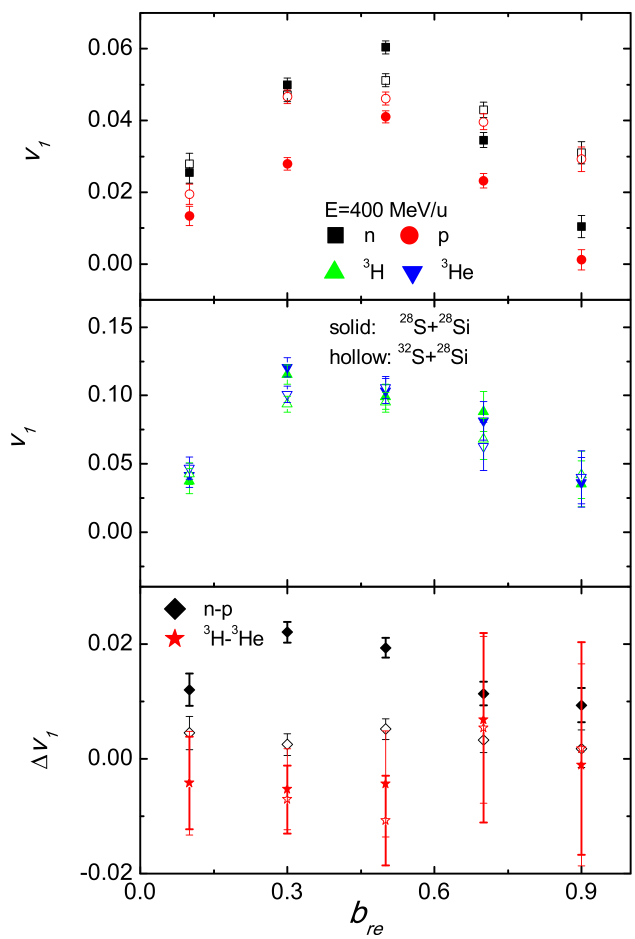

Fig. 8 (Color online) Same as in Fig. 7 but for 400 MeV/u

directed flows for neutron–proton and ^{3}H–^{3}He from ^{28}S + ^{28}Si collisions at low energies are noticeably equal and relatively larger under intermediate impact parameters, but reach zero for ^{32}S + ^{28}Si reactions, and only the difference in directed flows for neutron–proton from high-energy ^{28}S + ^{28}Si collisions is noticeable although much smaller than that from low-energy ^{28}S + ^{28}Si collisions. Thus, the differences of v_1 and the yield ratios for neutron–proton and ^{3}H–^{3}He under medium impact parameters are proposed as isospin observables for exotic nuclei. Further study on the quantitative relationship between a proton or neutron skin, as well as the yield ratio and difference in the directed flow, is being conducted.

References

1. Z.J. Wang, Z.Z. Ren, Elastic electron scattering on exotic light proton-rich nuclei. Phys. Rev. C **70**, 034303 (2004). https://doi.org/10.1103/PhysRevC.70.034303
2. S. Yoshida, H. Sagawa, Neutron skin thickness and equation of state in asymmetric nuclear matter. Phys. Rev. C **69**, 024318 (2004). https://doi.org/10.1103/PhysRevC.69.024318
3. A. Bhagwat, Y.K. Gambhir, Recently measured reaction cross sections with low energy fp-shell nuclei as projectiles: microscopic description. Phys. Rev. C **73**, 054601 (2006). https://doi.org/10.1103/PhysRevC.73.054601
4. J.G. Chen, X.Z. Cai, H.Y. Zhang et al., Proton halo or skin in the excited states of light nuclei. Chin. Phys. Lett. **20**(7), 1021–1024 (2003). https://doi.org/10.1088/0256-307X/20/7/314
5. C.J. Horowitz, S.J. Pollock, P.A. Souder et al., Parity violating measurements of neutron densities. Phys. Rev. C **63**, 025501 (2001). https://doi.org/10.1103/PhysRevC.63.025501
6. P. Danielewicz, Surface symmetry energy. Nucl. Phys. A **727**, 233 (2005). https://doi.org/10.1016/j.nuclphysa.2003.08.001
7. M. Liu, N. Wang, Z.X. Li et al., Neutron skin thickness of nuclei and effective nucleon–nucleon interactions. Chin. Phys. Lett. **23**(4), 804 (2006). https://doi.org/10.1088/0256-307X/23/4/012
8. K. Bennaceur, F. Nowacki, J. Okolowicz et al., Study of the ^{7}Be(p, γ)^{8}B and ^{7}Li(n, γ)^{8}Li capture reactions using the shell model embedded in the continuum. Nucl. Phys. A **651**, 289 (1999). https://doi.org/10.1016/S0375-9474(99)00133-5

9. K. Kaneko, Y. Sun, G. Angelis, Enhancement of high-spin collectivity in N = Z nuclei by the isoscalar neutron–proton pairing. Nucl. Phys. A **957**, 144 (2017). https://doi.org/10.1016/j.nuclphysa.2016.08.007
10. Z.H. Sun, Q. Wu, Z.H. Zhao et al., Resonance and continuum Gamow shell model with realistic nuclear forces. Phys. Lett. B **769**, 227–232 (2017). https://doi.org/10.1016/j.physletb.2017.03.054
11. I. Tanihata, H. Hamagaki, O. Hashimoto et al., Measurements of interaction cross sections and nuclear radii in the light p-shell region. Phys. Rev. Lett. **55**, 2676 (1985). https://doi.org/10.1103/PhysRevLett.55.2676
12. D.Q. Fang, W. Guo, C.W. Ma et al., Examining the exotic structure of the proton-rich nucleus ^{23}Al. Phys. Rev. C **76**, 031601(R) (2007). https://doi.org/10.1103/PhysRevC.76.031601
13. X.F. Li, D.Q. Fang, Y.G. Ma, Determination of the neutron skin thickness from interaction cross section and chargechanging cross section for B, C, N, O, F isotopes. Nucl. Sci. Tech. **27**, 71 (2016). https://doi.org/10.1007/s41365-016-0064-z
14. Y.D. Song, H.L. Wei, C.W. Ma et al., Improved FRACS parameterizations for cross sections of isotopes near the proton drip line in projectile fragmentation reactions. Nucl. Sci. Tech. **29**, 96 (2018). https://doi.org/10.1007/s41365-018-0439-4
15. B.A. Li, C.M. Ko, Isospin dependence of collective flow. Nucl. Phys. A **654**, 797c–802c (1999). https://doi.org/10.1016/S0375-9474(00)88549-8.
16. L.W. Chen, F.S. Zhang, Z.Y. Zhu, Isospin effects on rotational flow in intermediate energy heavy ion collisions. Phys. Rev. C **61**, 067601 (2000). https://doi.org/10.1103/PhysRevC.61.067601
17. V.N. Russkikh, Y.B. Ivanov, Collective flow in heavy-ion collisions for E_{lab} = 1–160 GeV/nucleon. Phys. Rev. C **74**, 034904 (2006). https://doi.org/10.1103/PhysRevC.74.034904
18. Z.Q. Feng, Dynamics of strangeness and collective flows in heavy-ion collisions near threshold energies. Nucl. Phys. A **919**, 32–45 (2013). https://doi.org/10.1016/j.nuclphysa.2013.10.005
19. H.Y. Zhang, W.Q. Shen, Y.G. Ma et al., Directed and elliptic flows in ^{40}Ca + ^{40}Ca and ^{112}Sn + ^{112}Sn collisions. Eur. Phys. J. A **15**, 399–404 (2002). https://doi.org/10.1140/epja/i2002-10043-7
20. S. Gautam, A.D. Sood, R.K. Puri et al., Isospin effects in the disappearance of flow as a function of colliding geometry. Phys. Rev. C **83**, 014603 (2011). https://doi.org/10.1103/PhysRevC.83.014603
21. X.Y. Sun, D.Q. Fang, Y.G. Ma et al., Neutron/proton ratio of nucleon emissions as a probe of neutron skin. Phys. Lett. B **682**, 396–400 (2010). https://doi.org/10.1016/j.physletb.2009.11.031
22. J.Y. Liu, Q. Zhao, S.J. Wang et al., Entrance channel dependence and isospin dependence of preequilibrium nucleon emission in intermediate energy heavy ion collisions. Nucl. Phys. A **687**, 475–485 (2001). https://doi.org/10.1016/S0375-9474(00)00581-9
23. X.C. Zhang, B.A. Li, L.W. Chen et al., Impact parameter dependence of the double neutron/proton ratio of nucleon emissions in isotopic reaction systems. Chin. Phys. Lett. **26**(5), 052502 (2009). https://doi.org/10.1088/0256-307X/26/5/052502
24. H.L. Liu, G.C. Yong, D.H. Wen, Probing the momentum dependence of the symmetry potential by the free n/p ratio of pre-equilibrium emission. Phys. Rev. C **91**, 024604 (2015). https://doi.org/10.1103/PhysRevC.91.024604
25. D. Theriault, J. Gauthier, F. Grenier et al., Neutron-to-proton ratios of quasiprojectile and midrapidity emission in the ^{64}Zn + ^{64}Zn reaction at 45 MeV/nucleon. Phys. Rev. C **74**, 051602(R) (2006). https://doi.org/10.1103/PhysRevC.74.051602
26. Y.X. Zhang, M.B. Tsang, Z.X. Li et al., Constraints on nucleon effective mass splitting with heavy ion collisions. Phys. Lett. B **732**, 186–190 (2014). https://doi.org/10.1016/j.physletb.2014.03.030
27. W.J. Xie, J. Su, L. Zhu et al., Neutron–proton effective mass splitting in a Boltzmann–Langevin approach. Phys. Rev. C **88**, 061601(R) (2013). https://doi.org/10.1103/PhysRevC.88.061601
28. J. Su, L. Zhu, C.Y. Huang et al., Correlation between symmetry energy and effective κ-mass splitting with an improved isospin- and momentum-dependent interaction. Phys. Rev. C **94**, 034619 (2016). https://doi.org/10.1103/PhysRevC.94.034619
29. M. Yu, K.J. Duan, S.S. Wang et al., A nuclear density probe: isobaric yield ratio difference. Nucl. Sci. Tech. **26**, S20503 (2015). https://doi.org/10.13538/j.1001-8042/nst.26.S20503
30. B.A. Li, B.J. Cai, L.W. Chen et al., Isospin dependence of nucleon effective masses in neutron-rich matter. Nucl. Sci. Tech. **27**, 141 (2016). https://doi.org/10.1007/s41365-016-0140-4
31. J. Aichelin, "Quantum" molecular dynamics: a dynamical microscopic n-body approach to investigate fragment formation and the nuclear equation of state in heavy ion collisions. Phys. Rep. **202**, 233–360 (1991). https://doi.org/10.1016/0370-1573(91)90094-3
32. L.W. Chen, F.S. Zhang, G.M. Jin, Analysis of isospin dependence of nuclear collective flow in an isospin-dependent quantum molecular dynamics model. Phys. Rev. C **58**, 2283 (1998). https://doi.org/10.1103/PhysRevC.58.2283
33. Y.G. Ma, W.Q. Shen, Z.Y. Zhu, Collective motion of reverse-reaction system in the intermediate-energy domain via the quantum-molecular-dynamics approach. Phys. Rev. C **51**, 1029 (1995). https://doi.org/10.1103/PhysRevC.51.1029
34. Y.X. Zhang, Z.X. Li, C.S. Zhou et al., Effect of isospin-dependent cluster recognition on the observables in heavy ion collisions. Phys. Rev. C **85**, 051602(R) (2012). https://doi.org/10.1103/PhysRevC.85.051602
35. G.A. Lalazissis, A.R. Farhan, M.M. Sharma, Light nuclei near neutron and proton drip lines in relativistic mean-field theory. Nucl. Phys. A **628**, 221–254 (1998). https://doi.org/10.1016/S0375-9474(97)00630-1